



Far-ultraviolet to Near-infrared Observations of SN 2023ixf: A High-energy Explosion Engulfed in Complex Circumstellar Material

Rishabh Singh Teja^{1,2}, Avinash Singh³, Judhajeet Basu^{1,2}, G. C. Anupama¹, D. K. Sahu¹, Anirban Dutta^{1,2}, Vishwajeet Swain⁴, Tatsuya Nakaoka³, Utkarsh Pathak⁴, Varun Bhalerao⁴, Sudhanshu Barway¹, Harsh Kumar⁴,

Nayana A. J.¹, Ryo Imazawa⁵, Brajesh Kumar⁶, and Koji S. Kawabata³

¹ Indian Institute of Astrophysics, II Block, Koramangala, Bengaluru-560034, Karnataka, India; rishabh.teja@iiap.res.in, rsteja001@gmail.com

² Pondicherry University, R.V. Nagar, Kalapet, Pondicherry-605014, UT of Puducherry, India

³ Hiroshima Astrophysical Science Center, Hiroshima University, Higashi-Hiroshima, Hiroshima 739-8526, Japan; avinash21292@gmail.com

⁴ Department of Physics, Indian Institute of Technology Bombay, Powai, Mumbai 400076, India

⁵ Department of Physics, Graduate School of Advanced Science and Engineering, Hiroshima University, Kagamiyama, 1-3-1 Higashi-Hiroshima, Hiroshima 739-8526, Japan

⁶ Aryabhata Research Institute of Observational Sciences, Manora Peak, Nainital-263001, Uttarakhand, India

Received 2023 June 16; revised 2023 July 19; accepted 2023 August 8; published 2023 August 25

Abstract

We present early-phase panchromatic photometric and spectroscopic coverage spanning the far-ultraviolet to near-infrared regime of the nearest hydrogen-rich core-collapse supernova (SN) in the last 25 yr, SN 2023ixf. We observe early “flash” features in the optical spectra due to confined dense circumstellar material (CSM). We observe high-ionization absorption lines (Fe II, Mg II) in the ultraviolet spectra from very early on. We also observe a multi-peaked emission profile of H α in the spectrum beginning at ~ 16 days, which indicates ongoing interaction of the SN ejecta with a preexisting shell-shaped CSM having an inner radius of ~ 75 au and an outer radius of ~ 140 au. The shell-shaped CSM is likely a result of enhanced mass loss ~ 35 – 65 yr before the explosion assuming a standard red supergiant wind. The UV spectra are dominated by multiple highly ionized narrow absorption and broad emission features from elements such as C, N, O, Si, Fe, and Ni. Based on early light-curve models of Type II SNe, we infer that the nearby dense CSM confined to $7 \pm 3 \times 10^{14}$ cm (~ 45 au) is a result of enhanced mass loss ($10^{-3.0 \pm 0.5} M_{\odot} \text{ yr}^{-1}$) two decades before the explosion.

Unified Astronomy Thesaurus concepts: Core-collapse supernovae (304); Type II supernovae (1731); Observational astronomy (1145); Extreme ultraviolet astronomy (2170); Near infrared astronomy (1093)

Supporting material: data behind figure

1. Introduction

Massive stars ($\gtrsim 8 M_{\odot}$) that meet their fate with explosive phenomena are termed core-collapse supernovae (CCSNe). They are either hydrogen-rich (Type II) or hydrogen-poor (Type Ib, Ic; Filippenko 1997). Recent advancements in all-sky surveys (e.g., the Zwicky Transient Facility, ZTF, and ATLAS) have made it possible to discover young supernovae (SNe) when rapid changes occur in their light curves, spectral energy distribution (SED), and spectral evolution apart from increasing brightness (Khazov et al. 2016; Bruch et al. 2023). The early evolution of a good fraction ($>36\%$) of Type II SNe is dominated by narrow emission features associated with confined dense circumstellar material (CSM; Bruch et al. 2021, 2023). The characteristics of the nearby dense CSM are visible in the spectral sequence as “flash” features consisting of narrow high-ionization lines that last a few to several days depending on the radius and density of the CSM (Gal-Yam et al. 2014; Yaron et al. 2017; Jacobson-Galán et al. 2022). The flash features are caused by the ionizing photons that result when the shock breaks out from the stellar surface and flashes/ionizes the nearby CSM. Some authors (Kochanek 2019; Jacobson-Galán et al. 2022) have noted that the ionization from shock breakout lasts for a few hours only, and, to get prolonged

flash features, another photon source is required, such as ejecta–CSM interaction. The earliest detailed time series observations of “flash spectroscopy” were observed for SN 2013fs (Yaron et al. 2017). The confined CSM ($< 10^{15}$ cm) of SN 2013fs was indicated by the disappearance of flash features, and it was consistent with the radio nondetection (Yaron et al. 2017). It was argued that this could only result if the progenitor had undergone a short-lived episode of enhanced mass loss just a few years before the explosion. Even though the rise of all-sky surveys has led to an order-of-magnitude increase in the early detection (and follow-up) of such events (Blagorodnova et al. 2018; Nicholl 2021), the physics behind the specifics of such interaction and the origins of CSM are still not definitively understood, and the associated observables, such as light curves, are not very well constrained (Fuller 2017; Wu & Fuller 2021; Dessart & Hillier 2022; Ko et al. 2022; Moriya et al. 2023).

The CCSNe have been studied extensively in optical and near-infrared (NIR) regimes, but extensive studies in the ultraviolet (UV) regime are still limited (Brown et al. 2007; Pritchard et al. 2014; Vasylyev et al. 2023). The crucial aspect of the observational investigation in the UV is the requirement of observation from space-based missions (Vasylyev et al. 2022; Bostroem et al. 2023a), for which scheduling time-disruptive target-of-opportunity (ToO) observations is not rapid for a majority of missions. The flux in UV declines very rapidly, requiring prompt observations and follow-ups. The UV emission from young CCSNe allows the investigation of hot



Original content from this work may be used under the terms of the [Creative Commons Attribution 4.0 licence](https://creativecommons.org/licenses/by/4.0/). Any further distribution of this work must maintain attribution to the author(s) and the title of the work, journal citation and DOI.

and dense ejecta and/or the presence of CSM when the photosphere is located in the outer layers of the progenitor star (Bufano et al. 2009). Many Type II SNe show a nearly featureless early optical spectral sequence, unlike the far-UV (FUV) and near-UV (NUV), which showcase a plethora of metal features. The detection of these features can be used to determine the composition of the outer envelope of the pre-SN star, the temperature of the outer layers of the ejecta, or the CSM and its characteristics (Dessart et al. 2022; Bostroem et al. 2023a).

On 2023 May 19 17:27:15.00 UT (JD 2,460,084.23), SN 2023ixf was discovered in the galaxy M101 at ~ 14.9 mag in the “clear” filter (Itagaki 2023) and classified as a Type II SN (Perley & Gal-Yam 2023; Teja et al. 2023a). The pre-discovery photometry from ZTF and other Transient Name Server (TNS) alerts provides tight constraints on the explosion epoch. Using the last nondetection (JD 2,460,083.31) and first detection (JD 2,460,083.32; Chufarin et al. 2023), we find the explosion epoch, $t_{\text{exp}} = \text{JD } 2,460,083.315 \pm 0.005$, which has been used throughout this work. We note that the last nondetection used is not very deep (>18 mag), and if we consider the deeper nondetection (>20.5 mag; Mao et al. 2023) on JD 2,460,083.16, the explosion epoch has a marginal change (of ~ 0.08 day) to JD 2460083.235.

Several professional and amateur astronomers have followed up on SN 2023ixf, as it is one of the nearest CCSNe in the last 25 yr. Various time-domain groups across the globe have been monitoring it since soon after its discovery, and results based on the early observations have already been presented. The early-phase optical and NIR photometry and optical spectroscopy have been presented by Hosseinzadeh et al. (2023), Jacobson-Galan et al. (2023), and Yamanaka et al. (2023). The presence of flash features in the spectra and increased luminosity is interpreted as due to the presence of nitrogen-/helium-rich dense CSM and the interaction of SN ejecta with it (Jacobson-Galan et al. 2023; Yamanaka et al. 2023). Comparing the early light curve with the shock cooling emission (Hosseinzadeh et al. 2023) suggested that the progenitor of SN 2023ixf could be a red supergiant with radius $410 \pm 10 R_{\odot}$. The high-resolution spectroscopy revealed that the confined CSM is asymmetric (Smith et al. 2023). Preimaging data have been analyzed at the SN 2023ixf site in recent works, constraining the mass of the progenitor to between 12 and $17 M_{\odot}$ (Jencson et al. 2023; Kilpatrick et al. 2023; Pledger & Shara 2023; Soraisam et al. 2023). These estimates are well within the earlier detected CCSN progenitors (Smartt 2009; Van Dyk 2017).

This letter presents the panchromatic evolution of SN 2023ixf spanning FUV-to-NIR wavelengths during the first 3 weeks after its discovery. The flow of the paper is as follows. In Section 2, we estimate the distance to the host galaxy and its extinction and briefly describe the source of data acquisition and the reduction procedure. Further, we present our spectroscopic observation in Section 3, along with its analysis and modeling in different regimes. In Section 4, we describe the light-curve evolution and its early-phase analysis. We summarize and discuss this early-phase work in Section 5.

2. Observations and Data Reduction

Object SN 2023ixf exploded in the outer spiral arm of the host galaxy, M101, a face-on giant spiral galaxy that lies

comparatively close to the Local Group. Tikhonov et al. (2015) estimated a mean distance of 6.79 ± 0.14 Mpc ($\mu = 29.15 \pm 0.05$ mag) to M101 using the tip of the red giant branch method (Lee et al. 1993) with low uncertainty. Riess et al. (2022) used Cepheids to estimate a distance of 6.85 ± 0.15 Mpc ($\mu = 29.18 \pm 0.04$ mag). We adopt a mean distance of 6.82 ± 0.14 Mpc ($\mu = 29.17 \pm 0.04$ mag). The gas-phase metallicity was computed by Garner et al. (2022) using various H II regions in the galaxy and estimated an oxygen abundance of $12 + \log[\text{O}/\text{H}] \sim 8.7$ in the outer spiral arms of the galaxy, which is similar to solar metallicity (Asplund et al. 2009).

The Galactic reddening in the line of sight of SN 2023ixf inferred from the dust extinction map of Schlafly & Finkbeiner (2011) is $E(B - V) = 0.0077 \pm 0.0002$ mag. Using high-resolution data, Lundquist et al. (2023) computed the equivalent widths of the Na I D1 and D2 lines to be 0.118 and 0.169 Å, respectively. Using the relation from Poznanski et al. (2012), we infer a mean host reddening of $E(B - V) = 0.031 \pm 0.011$ mag using Na I D1 and D2. A total reddening of $E(B - V) = 0.039 \pm 0.011$ mag is adopted for SN 2023ixf, which is consistent with Smith et al. (2023).

2.1. Optical and NIR

We carried out broadband optical photometric observations in the Sloan Digital Sky Survey (SDSS) $u'g'r'i'z'$ filters beginning on 2023 May 20 UT using the robotic 0.7 m GROWTH-India telescope (GIT; Kumar et al. 2022) located at the Indian Astronomical Observatory (IAO), Hanle, India. Data were downloaded and processed with the standard GIT image processing pipeline described in Kumar et al. (2022). While standard processing was sufficient for the $g'r'i'z'$ bands, the u' -band data did not have enough stars for automated astrometry using `astrometry.net` (Lang et al. 2010) and further zero-point estimation. The zero-point was computed manually using several nonvariable SDSS stars available in the SN field for GIT images. Optical spectroscopic observations of SN 2023ixf were carried out using the HFOSC instrument mounted on the 2 m Himalayan Chandra Telescope (HCT), IAO (Prabhu 2014). The spectroscopic data were reduced in a standard manner using the packages and tasks in IRAF (for details, see Teja et al. 2023b).

The NIR data were obtained from the Hiroshima Optical and Near-Infrared Camera (Akitaya et al. 2014) mounted at the 1.5 m Kanata Telescope. The NIR data were reduced using standard procedures in IRAF, and the calibration was done using secondary stars from the Two Micron All Sky Survey catalog (Skrutskie et al. 2006).

2.2. Ultraviolet

On 2023 May 25 and 30 UT, SN 2023ixf was observed by the UltraViolet Imaging Telescope (UVIT; Kumar et al. 2012; Tandon et al. 2017) on board AstroSat in both imaging and spectroscopic modes. However, we could only use imaging data from May 30 for photometry, since the images from the earlier epoch are saturated. The spectra obtained at all epochs are of good quality and have been used for this study. We also triggered the UVIT for several ToO proposals. But, due to technical constraints, observations against our ToO request could be undertaken only on 2023 June 11. However, data obtained through ToO observations are immediately made

Table 1
Log of AstroSat Observations

ObsID	Date	Phase (days)	Instrument	Time (ks)
T05_108T01_ 9000005664	2023-05-25	+6.9	UVIT FUV SXT (FW)	7.32 7.90
T05_110T01_ 9000005672	2023-05-30	+11.9	UVIT FUV SXT (PC)	4.32 8.24
T05_116T01_ 9000005682 ^a	2023-06-11	+23.4	UVIT FUV SXT (PC)	3.48 15.24

Note.

^a Observation against our ToO.

public at the Indian Space Science Data Center (ISSDC) portal,⁷ and we have used the level 1 (raw) and level 2 (processed) data files available at ISSDC in this work. All of the UVIT observations are listed in Table 1. The UVIT observations were performed with the FUV F172M and F148W filters and gratings Grating1 and Grating2. These two gratings are mounted on the FUV filter wheel at positions F4 and F6, respectively (Kumar et al. 2012), and have perpendicular dispersion axes. The AstroSat-UVIT data were pre-processed with CCDLAB (Postma & Leahy 2017) following the steps described in Postma & Leahy (2021). Aperture photometry was performed using a 12 pixel (5'') aperture and calibrated following the procedures mentioned in Tandon et al. (2020). Spectral extraction and calibrations were performed manually following the procedure described in Tandon et al. (2020) and Dewangan (2021) using IRAF and python.

Beginning on 2023 May 21, SN 2023ixf was also monitored extensively by the Ultraviolet Optical Telescope (UVOT; Roming et al. 2005) on board the Neil Gehrels Swift Observatory (Gehrels et al. 2004). We utilize the publicly available data obtained from the Swift Archives.⁸ Photometry was performed using the UVOT data analysis software in HEASoFT, following the procedure described in Teja et al. (2022). To check for contamination, we looked at the archival Swift data of the host galaxy M101 (ID 00032081). The count rates at the SN site for an aperture similar to that used for the SN photometry are insignificant and comparable to the background. Being a very bright SN, most photometric data points were saturated. We checked the `saturate` and `sss_factor` flags from the output and discarded all of the saturated and unusable data points based on those flags. Spectroscopic data reduction for Swift UV-grism data was performed using the standard UVOTPY package, which includes the latest grism calibrations and corrections (Kuin 2014). Further, multiple spectra captured intranight were summed using the `uvotspec.sum_PHA-files` program in UVOTPY to increase the overall signal-to-noise ratio. The first two spectra separated by just 0.1 day showed intranight flux variability due to the rapid rise; hence, these two spectra were not summed. Around 1800 Å, a few spectra were contaminated by a strong source; therefore, we have considered the UVOT spectra beyond 1900 Å only.

2.3. X-Rays

Object SN 2023ixf was also observed with the Soft X-ray Telescope (SXT) covering the 0.3–7.0 keV energy band

(Singh et al. 2016, 2017) on board AstroSat (Singh et al. 2014). Data were obtained in photon counting (PC) and fast window (FW) modes over multiple orbits starting on May 25 (see Table 1). Orbit-wise level 2 data were downloaded from ISSDC and merged into a single cleaned event file using the standard Julia-based merger tool. Images, spectra, and light curves were produced using XSELECT v2.5a from HEASoFT 6.30.1. We do not obtain a statistically significant detection of the source in the data obtained from SXT observations, possibly due to low exposure times and pointing offsets. However, it was detected by other X-ray facilities, primarily in hard X-rays, with the following reports on ATel: NuSTAR (May 22; Grefenstette 2023), ART-XC (May 26 and 29; Mereminskiy et al. 2023), and Chandra (May 31; Chandra et al. 2023).

2.4. Other Data Sources

Being a nearby SN in one of the most well-observed host galaxies, M101, many amateur astronomers and professional observatories have monitored the SN. We supplemented our photometric data set with various detections and nondetections of SN 2023ixf from Astronomer’s Telegrams⁹ and TNS AstroNotes¹⁰ and include the magnitudes reported by Vannini & Julio (2023a), Vannini & Julio (2023b), Balam & Kendurkar (2023), Chufarin et al. (2023), D’Avanzo et al. (2023), Desrosiers et al. (2023), Filippenko et al. (2023), Fowler et al. (2023), Fulton et al. (2023), González-Carballo et al. (2023), Kendurkar & Balam (2023), Koltenbah (2023), Limeburner (2023), Mao et al. (2023), Perley & Irani (2023), Singh et al. (2023), Vannini (2023), and Zhang et al. (2023).

3. Spectral Analysis

3.1. Optical Spectra

The first optical spectrum of SN 2023ixf was obtained within 5 hr of discovery by the Liverpool Telescope (Perley & Gal-Yam 2023). Our spectroscopic follow-up with HCT began ~2 days after the explosion. We present the spectral data obtained from HCT until ~19 days after the explosion. The spectral sequence is shown in Figure 1. The early spectra, until ~10 days, show a prominent blue continuum with strong high-ionization emission features due to C IV, N IV, and He II, specifically, C IV 5805, C IV 7061, N IV 7115, He II 4540, He II 4686, and He II 5411 Å, along with the Balmer lines H α , H β , H γ , and H δ . Weak signatures of C III 5696, N III 4641, and He I 5876 Å are also seen in the spectra. The highly ionized emission features at ~2.1 days are well reproduced by a combination of a narrow Lorentzian (limited by the resolution) and an intermediate-width Lorentzian of 2500 km s⁻¹. Our findings during the flash ionization phase are similar to those reported in Bostroem et al. (2023b), Jacobson-Galan et al. (2023), Smith et al. (2023), and Yamanaka et al. (2023).

The strength of the narrow component fades gradually, in contrast to the intermediate-width component, as the SN flux rises in the optical wavelengths. Most of the flash features in our spectral sequence disappear after +7 days. In the spectrum of 7.9 days, we observe intermediate-width H α emission at ~1000 km s⁻¹, in addition to the emergence of a broad P Cygni feature with an absorption trough. This could possibly be due to a residual of ongoing interaction with the dense CSM

⁷ ISSDC Portal

⁸ Swift Archive Download Portal

⁹ Astronomer’s Telegrams

¹⁰ TNS AstroNote

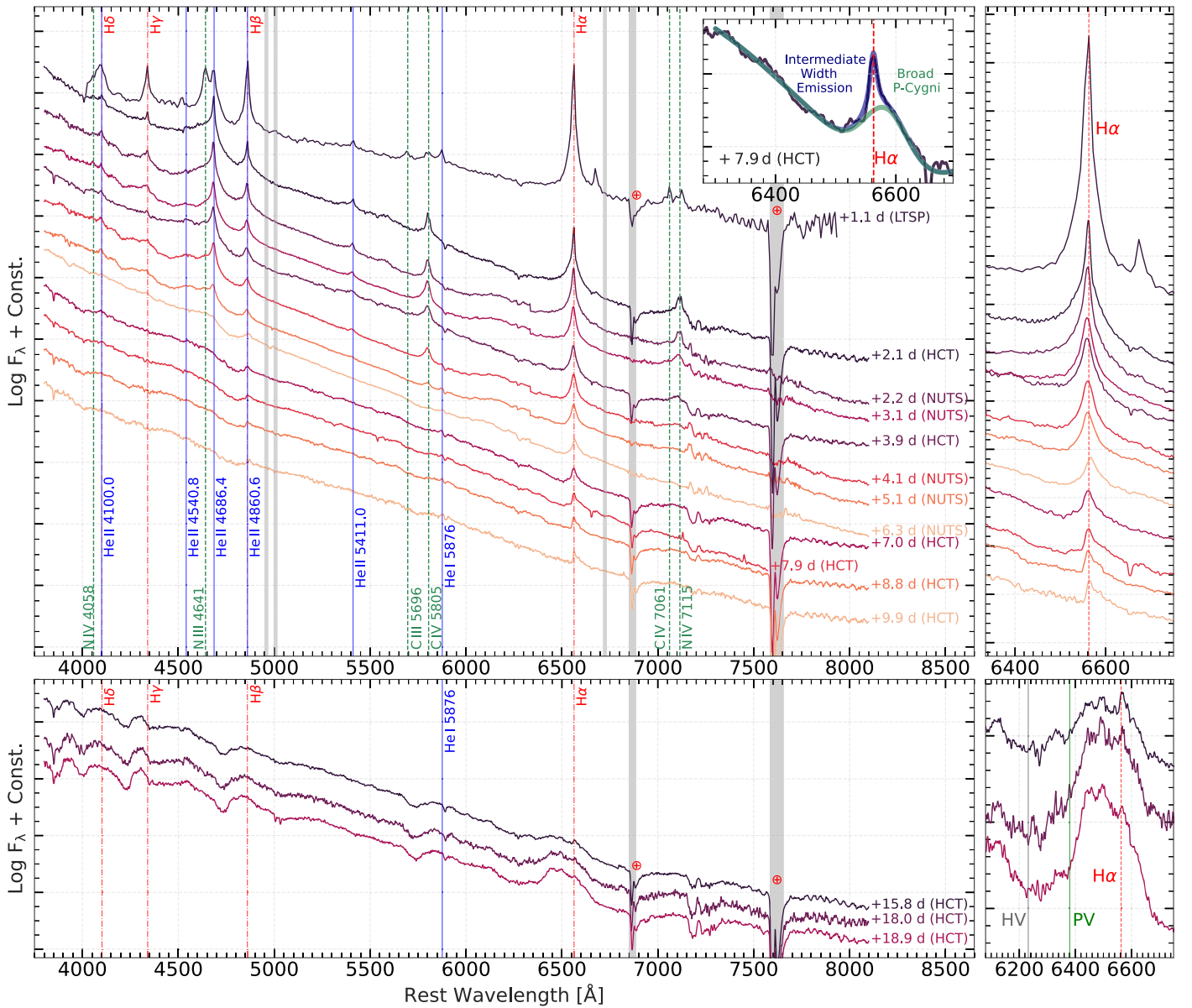


Figure 1. Optical spectral evolution for SN 2023ixf from HCT, Perley & Gal-Yam (2023), and Stritzinger et al. (2023). The spectra are corrected for the redshift of the host galaxy, M101, and the epochs are labeled with respect to our adopted explosion epoch. Top left: early-time spectral sequence of flash features in SN 2023ixf with line identification of high-ionization features and Balmer lines. The inset depicts the $H\alpha$ profile at +7.9 days having a broad P Cygni feature and intermediate-width Lorentzian emission. Top right: evolution of the line profile of $H\alpha$ during the flash phase. Bottom left: spectral sequence of SN 2023ixf during the photospheric phase. Bottom right: evolution of the multi-peaked emission profile of $H\alpha$ during the photospheric phase. Here HV and PV refer to the high- and photospheric-velocity components in the blueshifted absorption wing of $H\alpha$.

responsible for the flash-ionized phase. A similar profile is also seen for the $H\beta$ line. Beginning at ~ 16 days (bottom right panel of Figure 1), we observe a blueshifted multi-peaked emission profile of $H\alpha$ with a broad absorption feature that mimics the profile of a detached atmosphere (Jeffery & Branch 1990) and is an indication of the fast-moving SN shock encountering a low-density shell-shaped CSM (Pooley et al. 2002). The multi-peaked emission profile seen here is similar to the boxy emission profile seen during the photospheric phase in SN 2007od (Andrews et al. 2010), SN 2016gfy (Singh et al. 2019), and SN 2016esw (de Jaeger et al. 2018).

We observe two absorption troughs blueward of $H\alpha$ at 8000 (photospheric velocity, PV) and 15,000 (high velocity, HV) km s^{-1} in the spectrum of ~ 16 days. The HV feature, labeled

“Cachito” in the literature, could instead be due to the presence of Si II 6355 Å (Gutiérrez et al. 2017) in the blue wing of $H\alpha$. The estimated velocity ($\sim 5000 \text{ km s}^{-1}$) is lower than the PV if the feature is due to Si II. We also detect an analogous profile blueward of $H\beta$ with a similar velocity as seen in the $H\alpha$ profile, indicating that the feature is likely due to hydrogen only. However, the possibility of Si II blended with the HV feature of hydrogen cannot be ruled out altogether.

We estimated the PV using the minima of the absorption trough of $H\beta$, $H\gamma$, and He I 5876 Å. Although velocities estimated from Fe II act as a reliable tracer of PVs (Dessart & Hillier 2005), we used H and He line velocities, as they fairly resemble the PVs early in the photospheric phase (Faran et al. 2014). Using the ejecta velocities (PV and HV) estimated

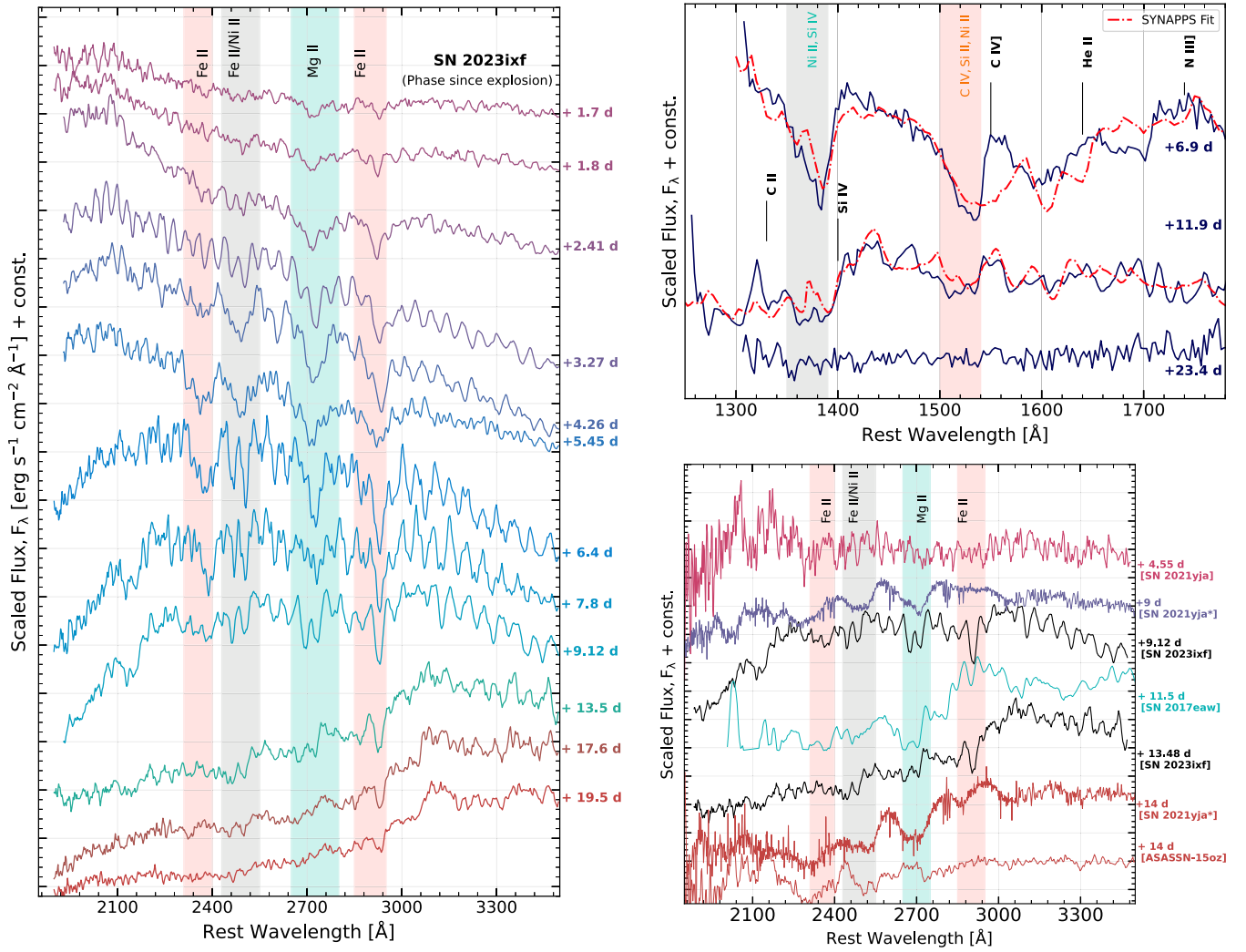


Figure 2. Left: NUV spectral evolution for SN 2023ixf obtained using Swift/UVOT. Top right: FUV spectral evolution obtained using Astrosat/UVIT and the SYNAPPS fit to the spectra of ~ 7 and ~ 12 days. Bottom right: spectral comparison of NUV spectra with other Type II SNe.

above, we compute an inner radius of ~ 75 au and an outer radius of ~ 140 au for the shell-shaped CSM encountered by the SN ejecta. Assuming a standard red super giant (RSG) wind velocity of 10 km s^{-1} (Smith 2014), the progenitor of SN 2023ixf likely experienced this enhanced mass loss ~ 35 – 65 yr before the explosion. If we consider the wind velocity of $\sim 115 \text{ km s}^{-1}$ inferred by Smith et al. (2023) using high-resolution optical spectra, we estimate that the mass-loss episode likely occurred ~ 3 – 6 yr before the explosion.

3.2. UV Spectra

We present the FUV (1250–1800 Å) and NUV (1900–3400 Å) spectral evolution of SN 2023ixf obtained with AstroSat and Swift, respectively, in Figure 2. Predominantly, the UV lines arise due to reemitted UV emission from highly ionized species created from the shock wave expanding into the ambient material (Williams 1967; Chevalier 1981; Fransson 1984; Chevalier & Fransson 1994). Along with the emission lines, the UV spectra are dominated by a large number of absorption lines from the interstellar matter in the Milky Way and the host galaxy due to highly ionized states of C, N, O, Si, etc. (Fransson 1984). Further, the UV spectra are not a simple continuum with isolated emissions and absorptions but a

continuous set of features having both emission and absorption features that are hard to identify at times (Pun et al. 1995; Dessart & Hillier 2010; Bostroem et al. 2023a). The UV spectra of Type II SNe are scarcely studied, particularly the FUV domain, which is largely unexplored. Object SN 1979C (Panagia et al. 1980) was the first Type II SN observed extensively in FUV, and SN 2022acko (Bostroem et al. 2023a) was the most recent one. For the present work, we restrict ourselves to describing the UV spectra qualitatively.

3.2.1. FUV Spectra

The FUV spectra of SN 2023ixf were obtained at three epochs of ~ 7 , ~ 12 , and ~ 23 days (see Table 1). The first spectrum for SN 2023ixf in the FUV is around the optical maximum (Section 4). In the spectrum of ~ 7 days, we observe two strong absorption bands in the wavelength regions 1340–1400 and 1500–1560 Å, which can be attributed to a blend of all or potentially a subset of following species Ni II 1370–1399, Si IV 1394–1403 Å lines, and C IV, Si II 1527, Ni II 1511 Å lines, respectively (Figure 2). Due to the low redshift of SN 2023ixf and with the available spectral resolution, it is difficult to discern whether the interstellar absorptions are either Galactic or due to the host galaxy. We further identify

Doppler-broadened emission features originating from C IV 1550, He II 1640, and N III] 1750 Å marked in the top right panel of Figure 2 similar to SN 1979C (Fransson 1984) and SN 2022acko (Bostroem et al. 2023a).

In the spectrum obtained at ~ 12 days, we continue to observe the two absorption bands but with diminishing depth. Other than the emission features observed in the spectrum of ~ 7 days, we find emission from C II 1335 Å, which could be blended earlier with strong absorption. The Si IV and N IV] could also be observed in the wavelength region 1400–1500 Å. As the flux continues to reduce in the FUV region, we see the disappearance of He II and N III] emission features. We corroborate the presence of these features by modeling the FUV spectrum at ~ 7 and ~ 12 days using the synthetic spectrum generation code SYNAPPS (Thomas et al. 2011). Many of the features in the spectra could be reproduced in the synthetic spectrum using the high-ionization (up to IV) species of He, C, N, O, S, Si, and Ni. More detailed spectral modeling with multiple elements is required to study these features extensively (Dessart & Hillier 2010; Bostroem et al. 2023a). As the SN evolves further, the high density of low-ionization lines of iron-group elements (especially Fe II and Fe III; Mazzali 2000) amplifies the line blanketing in the UV regime, as is evident in the FUV spectrum of ~ 23 days, which is noisy and featureless owing to the completely extinguished continuum flux. The complete extinction in FUV flux around +20 days is also evident in other Type II objects, such as SN 2021yja (Vasylyev et al. 2022), SN 2022wsp (Vasylyev et al. 2023), and SN 2022acko (Bostroem et al. 2023a).

3.2.2. NUV Spectra

The first NUV spectrum obtained at +1.7 days is the earliest NUV spectrum ever for any CCSN observed after SN 1987A. Contrary to the FUV, many Type II SNe have been observed in the NUV at multiple epochs. The NUV spectral coverage of SN 2023ixf is the most comprehensive ever up to +20 days after the explosion, with 12 spectra.

We observe weak and blended absorption features in the first spectrum in the wavelength range 2300–3000 Å. These absorption features continue to grow in strength and width and fully dominate the SN spectra at +6.4 days. The features arise particularly due to Fe II, Ni II, and Mg II species (Brown et al. 2007; Bostroem et al. 2023a; Vasylyev et al. 2023). The prominence of these absorption features weakens along with increased line blanketing, except for the feature present around 2900 Å, which is observed even in the last spectrum presented here, at +19.5 days.

The flux in the NUV started rising from the first epoch and reached a maximum ~ 5 days after the explosion as the SED transitioned to NUV. In the subsequent epochs, the NUV flux started declining and dropped to the level of the first epoch at around ~ 14 days. There is a significant drop in the flux between +5.5 and +6.4 days in the region of < 2200 Å, observed with the change in the shape of the SED, as is apparent in the left panel of Figure 2. This is probably due to the rapid cooling of the SN ejecta coupled with increased line blanketing in the UV wavelengths due to metal lines (Bufano et al. 2009). The effect of line blanketing in the region of < 3000 Å is much more prominent after +13.5 days, and it continues to dominate, with fluxes declining in this region.

The NUV spectrum of SN 2023ixf is compared with a few Type II SNe, such as ASASSN-15oz (Bostroem et al. 2019),

SN 2017eaw (Szalai et al. 2019), and SN 2021yja (Vasylyev et al. 2022), at similar epochs in the bottom right panel of Figure 2. Two spectra of SN 2021yja (+9 and +14 days) are from HST. All other spectra used for comparisons are from Swift/UVOT. Initially, the UV spectra of Type IIP SNe were thought to be homogeneous (Gal-Yam et al. 2008), but as their number grew, the dissimilarities became more evident (Bostroem et al. 2023a; Vasylyev et al. 2023). The absorption feature around 2700 Å arising from Mg II is observed in all SNe. The feature around 2900 Å was observed in SN 2023ixf, SN 2017eaw (IIL; Szalai et al. 2019), SN 2022wsp (IIP; Vasylyev et al. 2023), and SN 2022acko (IIP; Bostroem et al. 2023a). Detailed modeling for SN 2022acko revealed it to be an absorption window from the close-by Fe II, Cr II, and Ti II absorption complexes (Bostroem et al. 2023a). This absorption feature is also observed in SN 2021yja in the spectrum of +14 days.

The shape of the continuum is very similar prior to +10 days for SN 2021yja and SN 2023ixf. As the spectra evolve, a sharp cutoff in flux at < 3000 Å could be observed beyond +10 days in all SNe compared, indicating a significant line blanketing. Around +14 days, the differences in the spectra are very apparent, especially in ASASSN-15oz, where, in the spectrum below 2700 Å, we find strong emissions/absorptions, whereas others are devoid of flux comparable to regions beyond 2700 Å. Slightly higher flux beyond 3000 Å could indicate ongoing interaction (Vasylyev et al. 2022). More SNe need to be observed in the UV, specifically within the first 3 weeks of the explosion. This will be crucial in understanding the progenitor characteristics, its environment, and its effects on the early evolution and will aid in testing homogeneity in their spectra (Kulkarni et al. 2021; Bostroem et al. 2023a).

4. Light-curve Analysis

The multiband light curves based on observations from the various facilities described in Section 2 are shown in Figure 3. We converted all the pre- and postdiscovery public data to AB magnitude scale and included it with our data set using the transformations described in Blanton & Roweis (2007). The reported public data set is very helpful in putting tight constraints on the explosion epoch (Hosseinzadeh et al. 2023).

We do not see the fast-declining phase after maximum, the s_1 phase, usually attributed to the initial cooling phase postbreakout (Anderson et al. 2014), in the V -band light curve of SN 2023ixf. Instead, it declines very slowly for the initial few days, at $1.18_{-0.51}^{+0.49}$ mag 100 days $^{-1}$, right after it reaches a peak V -band magnitude of -18.06 ± 0.07 mag around ~ 5 days after explosion. The peak magnitude falls at the brighter end of Type II SNe. The peak V -band brightness is comparable with SN 2013by (Valenti et al. 2015) and SN 2014G (Terreran et al. 2016), which were classified as Type IIL, although with many similarities to the Type IIP subclass. Object SN 2014G also showed flash ionization features in early spectral evolution. While the initial decline of SN 2023ixf is inconsistent with that of Type IIL, its evolution at later phases has yet to be probed. Although the early spectra indicate interaction with a nearby dense CSM, SN 2023ixf is not extremely bright in the UV bands like Type IIn SNe.

The observed rise time of ~ 4 – 5 days is shorter than other normal Type II SNe, which, on average, take ~ 10 days to reach the peak (Valenti et al. 2016). We compare the $g - r$ color with similar events that showed flash features, such as SN 2013by

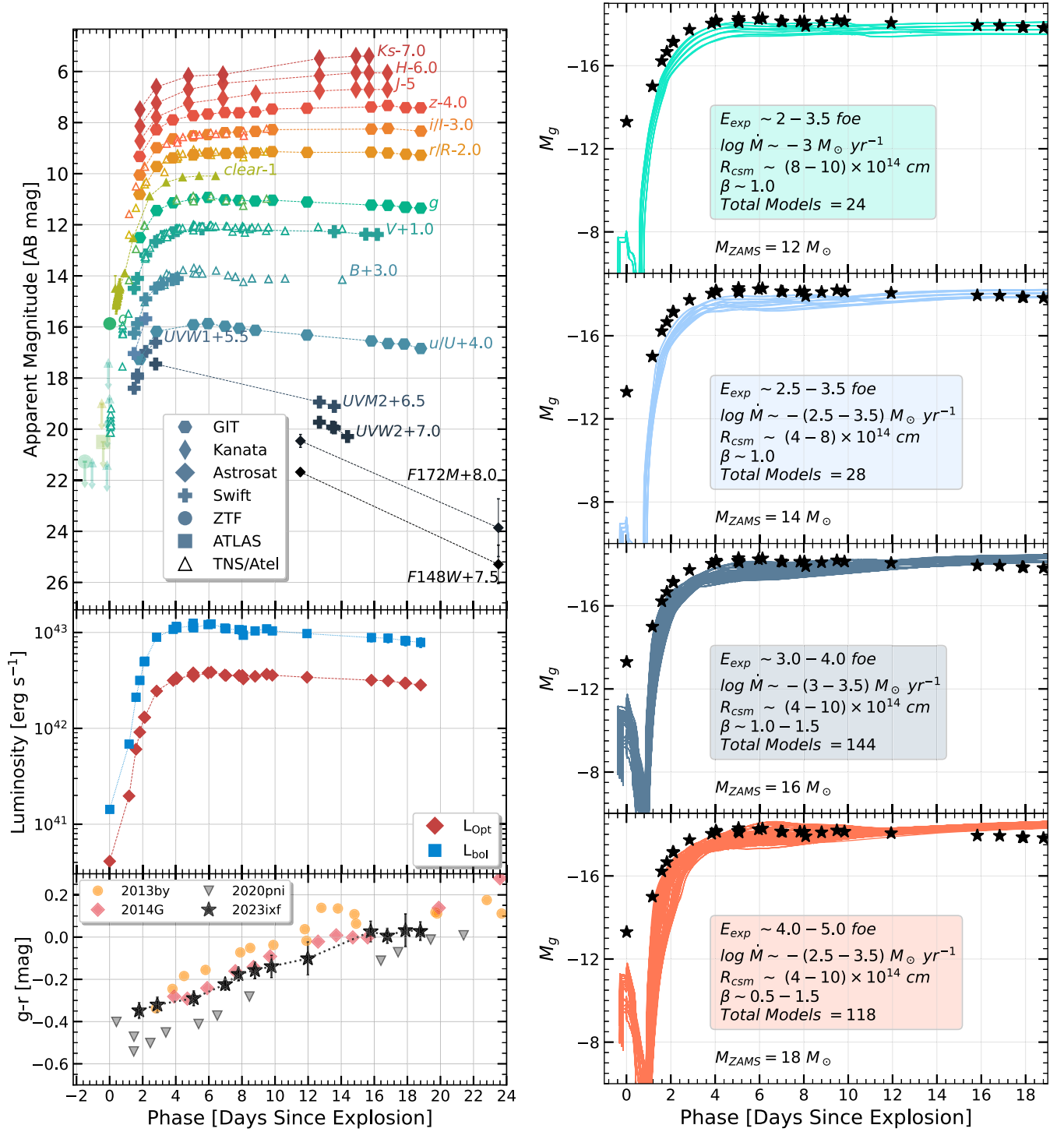


Figure 3. Left: multiband photometry is shown along with the data compiled from public sources. The middle panel shows the bolometric light-curve evolution. The bottom panel shows the color evolution of SN 2023ixf along with the other SNe with observed flash features. Right: best model light curves that could represent the g -band light-curve evolution of SN 2023ixf obtained out of a large sample of $>170,000$ models presented in Moriya et al. (2023) for different progenitor masses. The photometric data obtained using AstroSat, GIT, Kanata, and Swift are available as data behind the figure.

(The data used to create this figure are available.)

(Valenti et al. 2015; Black et al. 2017), SN 2014G (Terreran et al. 2016), and the bluest Type II SN 2020pni (Terreran et al. 2022). The color evolution is similar to these events for the initial ~ 20 days but slightly redder than SN 2020pni. The NIR light curves are also presented in Yamanaka et al. (2023) up to a week postexplosion. We show the evolution beyond that and

observe the flux increases in the NIR, possibly due to preexisting dust around the ejecta. The presence of pre-SN dust is also described in Neustadt et al. (2023).

The early prolonged flash features indicated the presence of a dense CSM around the progenitor. Recently, Moriya et al. (2023) provided a comprehensive set of grids for model light

curves that could shed light on the structure of CSM and its effects on the early light curve of interacting Type II SNe. In their work, a confined CSM is attached over a radius, R_0 , for five progenitors with mass ranging from 10 to 18 M_\odot . The CSM density structure follows Moriya et al. (2018), whereas the wind velocity, v_{wind} , at a distance r was taken to be in the form of

$$v_{\text{wind}}(r) = v_0 + (v_\infty - v_0) \left(1 - \frac{R_0}{r}\right)^\beta, \quad (1)$$

where v_0 and v_∞ are the initial wind velocity at the surface of the progenitor and the terminal velocity, respectively, and β is a wind structure parameter that determines the efficiency of wind acceleration.

These model light curves can be used to constrain the very early light-curve behavior of Type II SNe. Our work utilizes the well-sampled g -band light curve of SN 2023ixf to compare with the model grid of interacting Type II SNe generated by Moriya et al. (2023). We used the models with ^{56}Ni mass in the typical range of 0.01–0.04 M_\odot (Anderson et al. 2014). Furthermore, we found that the initial light curves are insensitive to the ^{56}Ni mass. We iterated over each parameter (E_{exp} , β , R_{CSM} , and \dot{M}) in succession, keeping others fixed with their full range for a single run. This procedure is repeated for 12, 14, 16, and 18 M_\odot progenitor models. We categorically reject models that show significant deviations from the observed light curves based on their peak luminosities and rise times. Subsequently, we do this for other parameters constraining the values for previous parameters. The best-fitting models for each progenitor are shown in Figure 3. We note that the slow early rise until day 2 is not captured by any of the models, and the later evolution is such that either the rise or plateau could be matched, but not the entire light curve. Since we are concerned about the initial rise, we do not probe it further; detailed hydrodynamical modeling specific to this particular event will be required to understand the entire light-curve evolution. Further, the degeneracy in the progenitor masses could not be lifted by these models, but these models give a very tight constraint on the radius of the outer CSM utilizing the rise times of the model light curves. The dense CSM is confined to $4.0\text{--}10.0 \times 10^{14}$ cm. Further, β varies from 0.5 to 1.5 depending on the progenitor mass, which is close to the typical values for RSGs ($\beta > 1$). The $\beta < 1$ value obtained for M_{ZAMS} would accelerate the winds slightly faster and cause less dense CSM in the vicinity, which is not the case for SN 2023ixf. The mass-loss rate is also slightly on the higher end ($10^{-3.0 \pm 0.5} M_\odot \text{ yr}^{-1}$). The average density of the CSM comes out to be $\sim 10^{-14} \text{ g cm}^{-3}$, which is in line with the values obtained in Bostroem et al. (2023b) but below the values inferred in Jacobson-Galan et al. (2023) obtained from the detailed spectral modeling. The mass-loss rates align with the density limits of CSM derived from the nondetection of radio emission (230 GHz) at early times (Berger et al. 2023). For a typical RSG ($\sim 500 M_\odot$), the above would translate to a mass loss of $\sim 14\text{--}18$ yr before the explosion. But, as seen in Smith et al. (2023), wind speeds measured using high-resolution early spectra are 1 order of magnitude higher than what is assumed in the model parameters, which would give an eruptive mass-loss timeline of around 2 yr before the explosion. However, wind acceleration cannot be ruled out. Another parameter that is tightly constrained by the models is the explosion energy. Only the models with explosion energies of more than 2.0 foe could

match the observed g -band flux. The explosion energy increases as the progenitor mass is increased. The explosion energy obtained is higher than for the usual Type II SNe.

In a recent work, Khatami & Kasen (2023) presented various light curves of transients arising from interacting SNe. These include the interaction of SN ejecta with no CSM to a very heavy CSM. Considering the latent space of luminosity and rise time presented in that work, we find that the light-curve evolution of SN 2023ixf (for the period presented in this work) appears to be similar to the model light curves for shock breakout in a light-CSM scenario. Comparing the rise times and peak luminosity of SN 2023ixf with the shock breakout happening inside the CSM, we find that it falls within $0.01 < M_{\text{CSM}} [M_\odot] < 0.1$. Using the parameters obtained from light-curve analysis, we get a CSM mass ranging from 0.001 to 0.03 M_\odot (assuming $v_{\text{wind}} = 10 \text{ km s}^{-1}$), where the upper limit is well within the range obtained from Khatami & Kasen (2023). It indicates that the mass-loss rate could have been even higher than $10^{-2.5} M_\odot \text{ yr}^{-1}$, as was also reported by Hiramatsu et al. (2023) and Jacobson-Galan et al. (2023).

5. Summary

This work presents an extensive set of early-phase observations for the closest CCSN in the last 25 yr, SN 2023ixf, which exploded in M101. The panchromatic observations covered wavelengths from the FUV to NIR regime using both ground- and space-based observatories. The multiband photometry spans the FUV to NIR, spanning up to ~ 23 days since the explosion. Light curves were compared with a large model light-curve grid to infer nearby dense CSM properties.

Detailed spectral coverage in the FUV, NUV, and optical during the first ~ 25 days after the explosion is presented, beginning within 2 days of the explosion. The lines due to Mg II and Fe II in the NUV and C III, C II, Si IV, and He II in the FUV were identified. The early (< 7 days) spectral sequence of SN 2023ixf indicates the presence of a dense CSM. Subsequently, there are no significant signatures, except for an intermediate-width emission feature of $\text{H}\alpha$ after +7 days. The high-resolution spectra presented by Smith et al. (2023) show the presence of an intermediate-width P Cygni profile during this phase, lasting for about a week, arising in the postshock, swept-up CSM shell. The line profile during the photospheric phase beginning at ~ 16 days shows a multi-peaked/boxy profile of $\text{H}\alpha$, indicating an ongoing CSM interaction with a shell-shaped CSM with an inner radius of ~ 75 au and an outer radius of ~ 140 au. Considering a standard RSG wind velocity, the progenitor likely experienced enhanced mass loss $\sim 35\text{--}65$ yr before the explosion. All of the above inferences from our multiwavelength observations indicate multifaceted circumstellar matter around the progenitor of SN 2023ixf.

The early-phase light curve of SN 2023ixf is influenced by the presence of dense nearby CSM, which was likely accumulated due to enhanced mass loss during the later stages of the progenitor's evolution. Object SN 2023ixf was found to have a very bright peak luminosity ($M_V \approx -18.1$ mag), much higher than the average luminosity for Type II SNe ($M_V \approx -16.7$ mag). Light curves were compared with a large model grid of interacting SNe with varied progenitor masses and CSM properties to infer the properties of the dense CSM in SN 2023ixf. Based on our comparison with light-curve models, the high luminosity is likely a mix of interaction with a confined CSM and an inherently energetic explosion. We

cannot conclusively decipher the weightage of the above components to the overall luminosity of SN 2023ixf; hence, further monitoring is required. We will continue to carry out the multiwavelength follow-up of SN 2023ixf.
















Acknowledgments

We thank the anonymous referee for an in-depth review that helped improve the manuscript. R.S.T. thanks Sergiy S. Vasylyev for providing the HST spectra of SN 2021yja. The GROWTH-India telescope (GIT) is a 70 cm telescope with a 0.7 field of view set up by the Indian Institute of Astrophysics (IIA) and the Indian Institute of Technology Bombay (IITB) with funding from the Indo-US Science and Technology Forum and the Science and Engineering Research Board, Department of Science and Technology, Government of India. It is located at the Indian Astronomical Observatory (IAO, Hanle). We acknowledge funding by the IITB alumni batch of 1994, which partially supports the operation of the telescope. Telescope technical details are available at <https://sites.google.com/view/growthindia/>. The HCT observations were made under our accepted ToO proposal HCT-2023-C2-P25. We thank the staff of IAO, Hanle, and CREST, Hosakote, that made these observations possible. The facilities at IAO and CREST are operated by the Indian Institute of Astrophysics, Bangalore. D. K.S. acknowledges the support provided by DST-JSPS under grant No. DST/INT/JSPS/P 363/2022. This research has made use of the High-Performance Computing (HPC) resources¹¹ made available by the Computer Center of the Indian Institute of Astrophysics, Bangalore. This research made use of REDPIPE¹² (Singh 2021), an assemblage of data reduction and analysis scripts written by A.S. This work uses the SXT and UVIT data from the AstroSat mission of the Indian Space Research Organisation (ISRO). The SN was observed through multiple ToO proposals, and the data were made public through the ISSDC data archive. We thank the SXT and UVIT payload operation centers for verifying and releasing the data via the ISSDC data archive and providing the necessary software tools. This work has also used software and/or web tools obtained from NASA's High Energy Astrophysics Science Archive Research Center (HEASARC), a service of the Goddard Space Flight Center and the Smithsonian Astrophysical Observatory. This work was also partially supported by a Leverhulme Trust Research Project Grant. This research also made use of the NASA/IPAC Extragalactic Database (NED¹³), which is funded by the National Aeronautics and Space Administration and operated by the California Institute of Technology.

Facilities: HCT, KT, Swift (UVOT), and AstroSat (UVIT and SXT).

Software: astropy (Astropy Collaboration et al. 2013, 2018), emcee (Foreman-Mackey et al. 2013), IRAF (Tody 1993), HEASoft (Nasa High Energy Astrophysics Science Archive Research Center (HEASARC), 2014), matplotlib (Hunter 2007), pandas (McKinney 2010), numpy (Harris et al. 2020), scipy (Virtanen et al. 2020), Jupyter-notebook (Kluyver et al. 2016), seaborn (Waskom 2021), and SYNAPPS (Thomas et al. 2011).

ORCID iDs

Rishabh Singh Teja  <https://orcid.org/0000-0002-0525-0872>
 Avinash Singh  <https://orcid.org/0000-0003-2091-622X>
 Judhajeet Basu  <https://orcid.org/0000-0001-7570-545X>
 G. C. Anupama  <https://orcid.org/0000-0003-3533-7183>
 D. K. Sahu  <https://orcid.org/0000-0002-6688-0800>
 Anirban Dutta  <https://orcid.org/0000-0002-7708-3831>
 Vishwajeet Swain  <https://orcid.org/0000-0002-7942-8477>
 Utkarsh Pathak  <https://orcid.org/0009-0002-7897-6110>
 Varun Bhalerao  <https://orcid.org/0000-0002-6112-7609>
 Sudhanshu Barway  <https://orcid.org/0000-0002-3927-5402>
 Harsh Kumar  <https://orcid.org/0000-0003-0871-4641>
 Nayana A. J.  <https://orcid.org/0000-0002-8070-5400>
 Ryo Imazawa  <https://orcid.org/0000-0002-0643-7946>
 Brajesh Kumar  <https://orcid.org/0000-0001-7225-2475>
 Koji S. Kawabata  <https://orcid.org/0000-0001-6099-9539>

References

- Akitaya, H., Moritani, Y., Ui, T., et al. 2014, *Proc. SPIE*, 9147, 914740
 Anderson, J. P., González-Gaitán, S., Hamuy, M., et al. 2014, *ApJ*, 786, 67
 Andrews, J. E., Gallagher, J. S., Clayton, G. C., et al. 2010, *ApJ*, 715, 541
 Asplund, M., Grevesse, N., Sauval, A. J., & Scott, P. 2009, *ARA&A*, 47, 481
 Astropy Collaboration, Price-Whelan, A. M., & Sipőcz, B. M. 2018, *AJ*, 156, 123
 Astropy Collaboration, Robitaille, T. P., Tollerud, E. J., et al. 2013, *A&A*, 558, A33
 Balam, D. D., & Kendurkar, M. 2023, *TNSAN*, 154, 1
 Berger, E., Keating, G. K., Margutti, R., et al. 2023, *ApJL*, 951, L31
 Black, C. S., Milisavljevic, D., Margutti, R., et al. 2017, *ApJ*, 848, 5
 Blagorodnova, N., Neill, J. D., Walters, R., et al. 2018, *PASP*, 130, 035003
 Blanton, M. R., & Roweis, S. 2007, *AJ*, 133, 734
 Bostroem, K. A., Dessart, L., Hillier, D. J., et al. 2023a, *ApJL*, 953, L18
 Bostroem, K. A., Pearson, J., Shrestha, M., et al. 2023b, arXiv:2306.10119
 Bostroem, K. A., Valenti, S., Horesh, A., et al. 2019, *MNRAS*, 485, 5120
 Brown, P. J., Dessart, L., Holland, S. T., et al. 2007, *ApJ*, 659, 1488
 Bruch, R. J., GalYam, A., Schulze, S., et al. 2021, *ApJ*, 912, 46
 Bruch, R. J., GalYam, A., Yaron, O., et al. 2023, *ApJ*, 952, 119
 Bufano, F., Immler, S., Turatto, M., et al. 2009, *ApJ*, 700, 1456
 Chandra, P., Maeda, K., Chevalier, R. A., Nayana, A. J., & Ray, A. 2023, *ATel*, 16073, 1
 Chevalier, R. A. 1981, *ApJ*, 251, 259
 Chevalier, R. A., & Fransson, C. 1994, *ApJ*, 420, 268
 Chufarin, V., Potapov, N., Ionov, I., et al. 2023, *TNSAN*, 150, 1
 D'Avanzo, P., Bianchetti, N., Bianchessi, M., et al. 2023, *TNSAN*, 153, 1
 de Jaeger, T., Galbany, L., Gutiérrez, C. P., et al. 2018, *MNRAS*, 478, 3776
 Desrosiers, J. B., Kendurkar, M. R., & Balam, D. D. 2023, *TNSAN*, 142, 1
 Dessart, L., & Hillier, D. J. 2005, *A&A*, 437, 667
 Dessart, L., & Hillier, D. J. 2010, *MNRAS*, 405, 2141
 Dessart, L., & Hillier, D. J. 2022, *A&A*, 660, L9
 Dessart, L., Prieto, J. L., Hillier, D. J., Kuncarayakti, H., & Hueichapan, E. D. 2022, *A&A*, 666, L14
 Dewangan, G. C. 2021, *JApA*, 42, 49
 Faran, T., Poznanski, D., Filippenko, A. V., et al. 2014, *MNRAS*, 442, 844
 Filippenko, A. V. 1997, *ARA&A*, 35, 309
 Filippenko, A. V., Zheng, W., & Yang, Y. 2023, *TNSAN*, 123, 1
 ForemanMackey, D., Hogg, D. W., Lang, D., & Goodman, J. 2013, *PASP*, 125, 306
 Fowler, M., Sienkiewicz, F., & Dussault, M. 2023, *TNSAN*, 143, 1
 Fransson, C. 1984, *A&A*, 133, 264
 Fuller, J. 2017, *MNRAS*, 470, 1642
 Fulton, M. D., Nicholl, M., Smith, K. W., et al. 2023, *TNSAN*, 124, 1
 GalYam, A., Arcavi, I., Ofek, E. O., et al. 2014, *Natur*, 509, 471
 GalYam, A., Bufano, F., Barlow, T. A., et al. 2008, *ApJL*, 685, L117
 Garner, R., Mihos, J. C., Harding, P., Watkins, A. E., & McGaugh, S. S. 2022, *ApJ*, 941, 182
 Gehrels, N., Chincarini, G., Giommi, P., et al. 2004, *ApJ*, 611, 1005
 González-Carballo, J., Farfán, R. G., Limón, F., et al. 2023, *TNSAN*, 136, 1
 Grefenstette, B. 2023, *ATel*, 16049, 1
 Gutiérrez, C. P., Anderson, J. P., Hamuy, M., et al. 2017, *ApJ*, 850, 89
 Harris, C. R., Millman, K. J., van der Walt, S. J., et al. 2020, *Natur*, 585, 357
 Hiramatsu, D., Tsuna, D., Berger, E., et al. 2023, arXiv:2307.03165

¹¹ <https://www.iap.res.in/?q=facilities/computing/nova>

¹² <https://github.com/sPaMFouR/RedPipe>

¹³ <https://ned.ipac.caltech.edu>

- Hosseinzadeh, G., Farah, J., Shrestha, M., et al. 2023, *ApJL*, **953**, L16
- Hunter, J. D. 2007, *CSE*, **9**, 90
- Itagaki, K. 2023, *TNSTR*, **2023**, 1
- Jacobson-Galán, W. V., Dessart, L., Jones, D. O., et al. 2022, *ApJ*, **924**, 15
- Jacobson-Galan, W. V., Dessart, L., Margutti, R., et al. 2023, arXiv:2306.04721
- Jencson, J. E., Pearson, J., Beasor, E. R., et al. 2023, *ApJL*, **952**, L30
- Jeffery, D. J., & Branch, D. 1990, in *Supernovae, Jerusalem Winter School for Theoretical Physics*, 6, ed. J. C. Wheeler, T. Piran, & S. Weinberg (Singapore: World Scientific), 149
- Kendurkar, M. R., & Balam, D. D. 2023, *TNSAN*, **129**, 1
- Khatami, D., & Kasen, D. 2023, arXiv:2304.03360
- Khazov, D., Yaron, O., GalYam, A., et al. 2016, *ApJ*, **818**, 3
- Kilpatrick, C. D., Foley, R. J., Jacobson-Galán, W. V., et al. 2023, *ApJL*, **952**, L23
- Kluyver, T., Ragan-Kelley, B., Pérez, F., et al. 2016, in *Positioning and Power in Academic Publishing: Players, Agents and Agendas*, ed. F. Loizides & B. Schmidt (Netherlands: IOS Press), 87
- Ko, T., Tsuna, D., Takei, Y., & Shigezuma, T. 2022, *ApJ*, **930**, 168
- Kochanek, C. S. 2019, *MNRAS*, **483**, 3762
- Koltenbah, B. 2023, *TNSAN*, **144**, 1
- Kuin, P. 2014, *UVOTPY: Swift UVOT Grism Data Reduction*, *Astrophysics Source Code Library*, ascl:1410.004
- Kulkarni, S. R., Harrison, F. A., Grefenstette, B. W., et al. 2021, arXiv:2111.15608
- Kumar, A., Ghosh, S. K., Hutchings, J., et al. 2012, *Proc. SPIE*, **8443**, 84431N
- Kumar, H., Bhalerao, V., Anupama, G. C., et al. 2022, *AJ*, **164**, 90
- Lang, D., Hogg, D. W., Mierle, K., Blanton, M., & Roweis, S. 2010, *AJ*, **139**, 1782
- Lee, M. G., Freedman, W. L., & Madore, B. F. 1993, *ApJ*, **417**, 553
- Limeburner, S. 2023, *TNSAN*, **128**, 1
- Lundquist, M., O'Meara, J., & Walawender, J. 2023, *TNSAN*, **160**, 1
- Mao, Y., Zhang, M., Cai, G., et al. 2023, *TNSAN*, **130**, 1
- Mazzali, P. A. 2000, *A&A*, **363**, 705
- McKinney, W. 2010, in *Proc. of the 9th Python in Science Conf.*, ed. S. van der Walt & J. Millman (SciPy), 56
- Mereminskiy, I. A., Lutovinov, A. A., Sazonov, S. Y., et al. 2023, *ATel*, **16065**, 1
- Moriya, T. J., Förster, F., Yoon, S. C., Gräfenner, G., & Blinnikov, S. I. 2018, *MNRAS*, **476**, 2840
- Moriya, T. J., Subrayan, B. M., Milisavljevic, D., & Blinnikov, S. I. 2023, *PASJ*, **75**, 634
- Nasa High Energy Astrophysics Science Archive Research Center (Heasarc) 2014, *HEASoft: Unified Release of FTOOLS and XANADU*, *Astrophysics Source Code Library*, ascl:1408.004
- Neustadt, J. M. M., Kochanek, C. S., & Rizzo Smith, M. 2023, arXiv:2306.06162
- Nicholl, M. 2021, *A&G*, **62**, 5
- Panagia, N., Vettolani, G., Boksenberg, A., et al. 1980, *MNRAS*, **192**, 861
- Perley, D., & Gal-Yam, A. 2023, *TNSCR*, **2023**, 1
- Perley, D. A., & Irani, I. 2023, *TNSAN*, **120**, 1
- Pledger, J. L., & Shara, M. M. 2023, *ApJL*, **953**, L14
- Pooley, D., Lewin, W. H. G., Fox, D. W., et al. 2002, *ApJ*, **572**, 932
- Postma, J. E., & Leahy, D. 2017, *PASP*, **129**, 115002
- Postma, J. E., & Leahy, D. 2021, *JApA*, **42**, 30
- Poznanski, D., Prochaska, J. X., & Bloom, J. S. 2012, *MNRAS*, **426**, 1465
- Prabhu, T. P. 2014, *PINSA*, **80**, 887
- Pritchard, T. A., Roming, P. W. A., Brown, P. J., Bayless, A. J., & Frey, L. H. 2014, *ApJ*, **787**, 157
- Pun, C. S. J., Kirshner, R. P., Sonneborn, G., et al. 1995, *ApJS*, **99**, 223
- Riess, A. G., Breuval, L., Yuan, W., et al. 2022, *ApJ*, **938**, 36
- Roming, P. W. A., Kennedy, T. E., Mason, K. O., et al. 2005, *SSRv*, **120**, 95
- Schlafly, E. F., & Finkbeiner, D. P. 2011, *ApJ*, **737**, 103
- Singh, A. 2021, *RedPipe: Reduction Pipeline*, *Astrophysics Source Code Library*, ascl:2106.024
- Singh, A., Kumar, B., Moriya, T. J., et al. 2019, *ApJ*, **882**, 68
- Singh, D., Visweswaran, G., Kagy, C., et al. 2023, *ATel*, **16054**, 1
- Singh, K. P., Stewart, G. C., Chandra, S., et al. 2016, *Proc. SPIE*, **9905**, 99051E
- Singh, K. P., Stewart, G. C., Westergaard, N. J., et al. 2017, *JAA*, **38**, 29
- Singh, K. P., Tandon, S. N., Agrawal, P. C., et al. 2014, *Proc. SPIE*, **9144**, 91441S
- Skrutskie, M. F., Cutri, R. M., Stiening, R., et al. 2006, *AJ*, **131**, 1163
- Smartt, S. J. 2009, *ARA&A*, **47**, 63
- Smith, N. 2014, *ARA&A*, **52**, 487
- Smith, N., Pearson, J., Sand, D. J., et al. 2023, arXiv:2306.07964
- Soraisam, M., Matheson, T., Andrews, J., et al. 2023, *TNSAN*, **139**, 1
- Stritzinger, M., Valerin, G., EliasRosa, N., et al. 2023, *TNSAN*, **145**, 1
- Szalai, T., Vinkó, J., Könyves-Tóth, R., et al. 2019, *ApJ*, **876**, 19
- Tandon, S. N., Postma, J., Joseph, P., et al. 2020, *AJ*, **159**, 158
- Tandon, S. N., Subramaniam, A., Girish, V., et al. 2017, *AJ*, **154**, 128
- Teja, R. S., Anupama, G., Sahu, D., & Kurre, M. 2023a, *TNSCR*, **2023**, 1
- Teja, R. S., Singh, A., Sahu, D. K., et al. 2022, *ApJ*, **930**, 34
- Teja, R. S., Singh, A., Sahu, D. K., et al. 2023b, arXiv:2306.10136
- Terreran, G., Jacobson-Galán, W. V., Groh, J. H., et al. 2022, *ApJ*, **926**, 20
- Terreran, G., Jerkstrand, A., Benetti, S., et al. 2016, *MNRAS*, **462**, 137
- Thomas, R. C., Nugent, P. E., & Meza, J. C. 2011, *PASP*, **123**, 237
- Tikhonov, N. A., Lebedev, V. S., & Galazutdinova, O. A. 2015, *AstL*, **41**, 239
- Tody, D. 1993, in *ASP Conf. Ser. 52, Astronomical Data Analysis Software and Systems II*, ed. R. J. Hanisch, R. J. V. Brissenden, & J. Barnes (San Francisco, CA: ASP), 173
- Valenti, S., Howell, D. A., Stritzinger, M. D., et al. 2016, *MNRAS*, **459**, 3939
- Valenti, S., Sand, D., Stritzinger, M., et al. 2015, *MNRAS*, **448**, 2608
- Van Dyk, S. D. 2017, *RSPTA*, **375**, 20160277
- Vannini, J. 2023a, *TNSAN*, **156**, 1
- Vannini, J. 2023b, *TNSAN*, **161**, 1
- Vannini, J. 2023, *TNSAN*, **141**, 1
- Vasylyev, S. S., Filippenko, A. V., Vogl, C., et al. 2022, *ApJ*, **934**, 134
- Vasylyev, S. S., Vogl, C., Yang, Y., et al. 2023, arXiv:2304.06147
- Virtanen, P., Gommers, R., Oliphant, T. E., et al. 2020, *NatMe*, **17**, 261
- Waskom, M. L. 2021, *JOSS*, **6**, 3021
- Williams, R. E. 1967, *ApJ*, **147**, 556
- Wu, S., & Fuller, J. 2021, *ApJ*, **906**, 3
- Yamanaka, M., Fujii, M., & Nagayama, T. 2023, arXiv:2306.00263
- Yaron, O., Perley, D. A., Gal-Yam, A., et al. 2017, *NatPh*, **13**, 510
- Zhang, K., Kennedy, D., Oostermeyer, B., Bloom, J., & Perley, D. A. 2023, *TNSAN*, **125**, 1